American Mineralogist, Volume 84, pages 130–137, 1999

Comparative high-pressure crystal chemistry of karrooite, $MgTi_2O_5$, with different ordering states

HEXIONG YANG* AND ROBERT M. HAZEN

Geophysical Laboratory and Center for High Pressure Research, Carnegie Institution of Washington, 5251 Broad Branch Road, NW, Washington, D.C. 20015-1305, U.S.A.

ABSTRACT

Two karrooite crystals, one with a disorder parameter (X = Ti content in the M1 site) of 0.070(5) and the other with X = 0.485(5), were mounted together in one diamond-anvil cell and studied by single-crystal X-ray diffraction at several pressures up to 7.51 GPa. The most noticeable effect of increasing cation disorder on the high-pressure behavior of the structure is to increase the compressibilities of the mean <M2-O> bond length from 0.00148(2) GPa^{-1} in the ordered sample to 0.00163(7) GPa^{-1} in the disordered one and decrease those of the mean <M1-O> bond length from 0.00243(5) to 0.00193(12) GPa^{-1}. These changes are responsible for the compressibility difference between the two phases observed by Hazen and Yang (1997). Both compressibilities of the mean <M-O> bond lengths and the octahedral volumes in two phases decrease linearly with increasing the Ti contents in the octahedral sites. All octahedra in two samples become less distorted as pressure increases, but those in the more disordered structure exhibit larger decreases in terms of the octahedral angle variance than the corresponding ones in the more ordered structure. The influence of pressure on the interatomic angles is small compared to the interatomic distances, suggesting that compression of the karrooite structure is controlled primarily by the bond-length shortening, rather than by bond-angle bending. The strong compressional anisotropy of the structure is a consequence of the differential compressibilities of the weaker Mg^{2+}-O and stronger Ti^{4+}-O bonds and the complex edge-sharing linkage involving the M1 and M2 octahedra.

INTRODUCTION

Effects of pressure on atomic order-disorder in crystalline phases have received much attention recently because of their great implications for materials science, geophysics, and solid-state physics (Hazen and Navrotsky 1996 and references therein). In particular, from high-pressure unit-cell dimension data, Hazen and Yang (1997) demonstrated that the cation disorder can increase the compressibility of karrooite ($MgTi_2O_5$) by as much as 6%, an order of magnitude greater than that predicted by bulk modulus-volume systematics. This result suggests that, in addition to structural and compositional factors, cation order-disorder also plays an important role in determining the elastic properties of crystalline phases. To provide a detailed crystal-chemical understanding of the high-pressure behavior of karrooite with different ordering states, we have performed a structural study on an ordered and a disordered karrooite crystal at various pressures up to 7.51 GPa using the comparative high-pressure method (Hazen 1993). The results reported in this paper are a part of our systematic investigations into the effects of pressure on atomic order-disorder in crystalline phases.

Karrooite is an end-member of the $MgTi_2O_5$-$FeTi_2O_5$ (ferropseudobrookite)-Fe_2TiO_5 (pseudobrookite) system and occurs in many volcanic and metamorphic rocks. It is also a constituent of refractory ceramics and magnetic materials. The cation order-disorder in $(Mg,Fe)Ti_2O_5$ compounds has been studied because of its strong effects on the crystal structure and high-temperature stabilization (Navrotsky 1975; Wechsler 1977; Wechsler and Navrotsky 1984; Wechsler and Von Dreele 1989; Brown and Navrotsky 1989). The crystal structure of karrooite was first refined by Lind and Housley (1972) based on the structural model for pseudobrookite (Pauling 1930). It consists of two crystallographically distinct, highly distorted octahedral sites, M1 and M2, with M1 larger and more distorted than M2. In general, the M1 site is predominately occupied by Mg and M2 by Ti, but a wide range of nonconvergent Mg-Ti order-disorder between M1 and M2 has been reported (Lind and Housley 1972; Smyth 1974; Virgo and Huggins 1975; Wechsler et al. 1976; Wechsler 1977; Brigatti et al. 1993). This order-disorder reaction is strongly temperature-dependent, with samples quenched from higher temperatures being substantially more disordered than those quenched from lower temperatures (Wechsler and Navrotsky 1984; Wechsler and Von Dreele 1989; Brown and Navrotsky 1989; Yang and Hazen 1998). The fully ordered and disordered struc-

* E-mail: yang@gl.ciw.edu

0003–004X/99/0102–0130$05.00

TABLE 1. Crystal data on karrooite annealed at 600 and 1400 °C at various pressures

Sample	*P* (GPa)	*a*(Å)	*b*(Å)	*c*(Å)	*V*(Å^3)	Refls. > 2σ(I)	R_{int}†	*Rw*†	*R*§
P600	0.00*	9.7131(5)	10.0190(4)	3.7363(5)	363.60(5)	193	0.019	0.024	
	0.49	9.7057(3)	10.0076(3)	3.7343(3)	362.71(2)				0.024
	1.03*	9.6944(3)	9.9924(2)	3.7316(3)	361.48(3)	187	0.021	0.025	0.025
	1.68	9.6821(4)	9.9760(3)	3.7287(3)	360.15(3)				
	2.16*	9.6739(4)	9.9651(3)	3.7265(3)	359.24(3)	191	0.021	0.027	0.028
	2.56	9.6678(4)	9.9562(3)	3.7240(3)	358.45(3)				
	3.22*	9.6540(4)	9.9387(3)	3.7218(3)	357.09(3)	190	0.022	0.025	0.024
	3.84	9.6442(4)	9.9249(3)	3.7193(3)	356.00(3)				
	4.34*	9.6349(4)	9.9143(3)	3.7168(3)	355.04(3)	195	0.022	0.029	0.030
	5.12	9.6205(4)	9.8944(4)	3.7133(3)	353.46(3)				
	6.20*	9.5992(3)	9.8667(3)	3.7085(2)	351.24(2)	190	0.022	0.028	0.028
	6.95	9.5857(3)	9.8503(3)	3.7050(2)	349.84(2)				
	7.51*	9.5754(3)	9.8352(3)	3.7029(3)	348.73(3)	192	0.023	0.032	0.032
P1400	0.00*	9.7602(5)	9.9796(4)	3.7479(3)	365.06(3)	171	0.021	0.021	0.022
	0.49	9.7511(3)	9.9686(3)	3.7454(2)	364.07(2)				
	1.03*	9.7392(3)	9.9539(3)	3.7426(2)	362.82(2)	173	0.023	0.024	0.025
	1.68	9.7255(4)	9.9385(3)	3.7392(2)	361.42(3)				
	2.16*	9.7166(3)	9.9275(3)	3.7369(2)	360.46(2)	171	0.022	0.021	0.022
	2.56	9.7092(4)	9.9186(4)	3.7351(3)	359.70(3)				
	3.22*	9.6949(6)	9.9022(3)	3.7313(5)	358.21(4)	180	0.025	0.027	0.028
	3.84	9.6827(3)	9.8879(2)	3.7288(2)	357.00(2)				
	4.34*	9.6737(3)	9.8769(3)	3.7271(2)	356.11(2)	183	0.028	0.032	0.031
	5.12	9.6580(3)	9.8584(4)	3.7228(3)	354.46(3)				
	6.20*	9.6327(3)	9.8302(3)	3.7177(2)	352.03(2)	174	0.028	0.035	0.033
	6.95	9.6189(3)	9.8146(3)	3.7143(2)	350.65(2)				
	7.51*	9.6080(3)	9.8024(3)	3.7114(3)	349.54(3)	184	0.026	0.034	0.035

* X-ray intensity data were collected at these pressures.
† Residual for internal agreement of symmetry equivalent reflections.
‡ $Rw = (\Sigma w(F_o - F_c)^2/\Sigma wF_o^2)^{0.5}$.
§ $R = \Sigma|F_o - F_c|/\Sigma|F_o|$.

tures are of the crystal-chemical forms of $(Mg)^{M1}(Ti_2)^{M2}O_5$ and $(Mg_{0.333}Ti_{0.667})^{M1}(Ti_{1.333}Mg_{0.667})^{M2}O_5$, respectively.

EXPERIMENTAL PROCEDURES

The two synthetic karrooite crystals (~0.10 mm × 0.10 mm × 0.04 mm), one of which was quenched rapidly from 600 °C and the other from 1400 °C (designated as P600 and P1400, respectively), examined here were previously studied by Hazen and Yang (1997) for comparative compressibilities and by Yang and Hazen (1998) for the effects of cation ordering on the crystal structure. The details of the crystal synthesis and quenching experiment were described by Yang and Hazen (1998). The disorder parameter, *X*, defined as the Ti content in the M1 site, is 0.070(5) for P600 and 0.485(5) for P1400. An Inconel 750× gasket of 0.26 mm in thickness was pre-indented to ~0.10 mm with two diamonds with the anvil faces of 0.70 mm. A 0.40 mm hole was drilled at the center of the pre-indented area and the two crystals were mounted together in a modified Merrill-Bassett diamond-anvil cell with a mixture of 4:1 methanol:ethanol as the pressure medium. Four small (~10 μm) ruby chips were included as the internal pressure calibrant (Mao et al. 1986), from which pressure was determined from the position of the R_1 laser-induced fluorescence peak, with an error of approximately 0.05 GPa.

A Picker four-circle diffractometer equipped with a Mo X-ray tube (β-filtered) was used for all X-ray diffraction measurements. The fixed-φ mode of data measurement (Finger and King 1978) was employed throughout the high-pressure experiments to maximize reflection accessibility and minimize attenuation by the diamond cell. Unit-cell parameters were determined by fitting the positions of 14–18 reflections with $20° < 2\theta < 35°$, following the procedure of King and Finger (1979). X-ray diffraction intensity data were collected on the basis of the *B*-centered lattice for all accessible reflections with $0° < 2\theta < 60°$ using ω scans of 1° width in step increments of 0.025° and 4 s per step counting time. The intensity data were measured at seven pressures up to 7.51 GPa. At 7.51 GPa, a set of intensity data with $0° < 2\theta < 30°$ were also collected for both crystals based on the primitive lattice to check if any reflections violated the symmetry of the *B*-centered lattice; no such reflections were detected. Digitized step data were integrated by the method of Lehmann and Larsen (1974) with background manually reset when necessary. Corrections were made for Lorentz and polarization effects, and for X-ray absorption by the crystal. In addition, corrections were made for absorption by the diamond and beryllium components of the pressure cell. Reflections having intensities greater than $2\sigma_I$ were considered as observed and were included in refinements, where σ_I is the standard deviation determined from the counting statistics.

The initial structural model of karrooite was taken from Yang and Hazen (1998). Least-squares refinements were carried out using an updated version of RFINE4 (Finger and Prince 1975) in space group *Bbmm*. Neutral atomic scattering factors, including anomalous dispersion corrections for Mg, Ti, and O, were taken from the *Interna-*

TABLE 2. Atomic positional and displacement parameters of karrooite annealed at 600 and 1400 °C at various pressures

			Pressure (GPa)						
Sample	Site	Loc.	0.00	1.03	2.16	3.22	4.34	6.20	7.51
P600	M1	*x*	0.8052(2)	0.8050(2)	0.8046(2)	0.8045(2)	0.8044(2)	0.8039(2)	0.8040(2)
		B	0.47(3)	0.51(3)	0.51(3)	0.50(3)	0.44(3)	0.39(3)	0.45(3)
	M2	*x*	0.1335(1)	0.1334(1)	0.1335(1)	0.1335(1)	0.1336(1)	0.1336(1)	0.1337(1)
		y	0.4332(1)	0.4332(1)	0.4333(1)	0.4333(1)	0.4334(1)	0.4333(1)	0.4334(1)
		B	0.38(2)	0.39(2)	0.39(2)	0.37(2)	0.35(2)	0.36(2)	0.42(2)
	O1	*x*	0.2188(4)	0.2195(4)	0.2197(4)	0.2197(4)	0.2202(5)	0.2210(5)	0.2215(5)
		B	0.54(6)	0.63(6)	0.56(6)	0.56(6)	0.47(7)	0.71(7)	0.65(7)
	O2	*x*	0.0459(3)	0.0459(3)	0.0466(3)	0.0461(3)	0.0465(3)	0.0464(3)	0.0467(3)
		y	0.8865(2)	0.8862(2)	0.8861(2)	0.8858(2)	0.8856(3)	0.8848(3)	0.8846(3)
		B	0.68(5)	0.71(5)	0.72(5)	0.73(5)	0.58(6)	0.60(6)	0.69(6)
	O3	*x*	0.3136(3)	0.3140(3)	0.3142(3)	0.3141(3)	0.3142(3)	0.3147(3)	0.3146(3)
		y	0.9374(2)	0.9380(2)	0.9377(3)	0.9377(3)	0.9379(3)	0.9382(3)	0.9379(3)
		B	0.56(4)	0.54(5)	0.55(5)	0.55(5)	0.54(6)	0.50(6)	0.50(6)
P1400	M1	*x*	0.8085(1)	0.8081(1)	0.8081(1)	0.8078(1)	0.8074(2)	0.8072(2)	0.8066(2)
		B	0.50(3)	0.55(3)	0.55(3)	0.51(3)	0.49(3)	0.49(3)	0.56(3)
	M2	*x*	0.1357(1)	0.1357(1)	0.1357(1)	0.1358(1)	0.1357(1)	0.1358(1)	0.1357(1)
		y	0.4369(1)	0.4368(1)	0.4367(1)	0.4368(1)	0.4367(1)	0.4365(1)	0.4367(1)
		B	0.55(2)	0.54(2)	0.55(2)	0.57(3)	0.48(2)	0.53(3)	0.54(3)
	O1	*x*	0.2341(4)	0.2338(4)	0.2339(4)	0.2342(4)	0.2339(5)	0.2344(6)	0.2354(5)
		B	1.16(8)	1.03(8)	1.03(7)	1.14(8)	0.89(8)	0.71(8)	0.74(8)
	O2	*x*	0.0467(3)	0.0471(3)	0.0472(3)	0.0473(3)	0.0474(3)	0.0474(4)	0.0471(4)
		y	0.8841(3)	0.8832(3)	0.8832(2)	0.8827(3)	0.8828(3)	0.8829(4)	0.8821(4)
		B	0.83(5)	0.87(5)	0.82(5)	0.94(6)	0.68(6)	0.66(7)	0.82(7)
	O3	*x*	0.3110(3)	0.3109(3)	0.3112(3)	0.3125(3)	0.3123(3)	0.3128(4)	0.3137(4)
		y	0.9304(3)	0.9303(3)	0.9301(2)	0.9312(3)	0.9307(3)	0.9310(4)	0.9310(3)
		B	0.67(6)	0.86(6)	0.81(5)	0.80(6)	0.70(6)	0.69(7)	0.66(7)

Note: The following constraints apply to some atomic positional coordinates: $y = ¼$ for M1 and O1; $z = 0$ for all atoms.

tional Tables for X-ray Crystallography (Ibers and Hamilton 1974). For all high-pressure structure refinements, the Mg-Ti occupancies at the M1 and M2 sites for both samples were assumed to be the same as those determined from the room-pressure data collected without the diamond-anvil cell (Yang and Hazen 1998). Anisotropic refinements were made for all data sets of two samples. Weighting schemes were based on $w = [\sigma^2(F) + (pF)^2]^{-1}$, where p is adjusted to ensure that the errors were normally distributed through probability plot analysis (Ibers and Hamilton 1974). Type II isotropic extinction corrections (Becker and Coppens 1975) were applied in the refinements. Unit-cell dimensions and final refinement statistics are given in Table 1. Atomic positional and isotropic displacement parameters are in Table 2; selected interatomic distances, polyhedral volumes, and distortion indices are in Table 3 and selected interatomic angles are in Table 4.

RESULTS AND DISCUSSION

The most noticeable effect of increasing cation disorder on the high-pressure behavior of the karrooite structure is to increase the compressibility of the M2 octahedron and decrease that of the M1 octahedron, giving rise to a more isotropically compressible structure. All M1 and M2 octahedral volumes in P600 and P1400 decrease linearly as pressure increases; the bulk moduli of the M1 and M2 octahedra in P600 are 172(4) and 250(7) GPa, respectively, whereas those in P1400 are 214(18) and 237(13) GPa. These values do not appear to relate directly to the octahedral sizes, given that the M1 and M2 octahedra in P1400 at room pressure have similar volume values (Table 3). Yet, they are a linear function of the Ti contents in the octahedral sites (Fig. 1): K(GPa) = 168(4) + 88(6)X. This relationship is understandable because the Ti^{4+}-O bond is stronger than the Mg^{2+}-O bond. Estimated bulk moduli for an octahedron occupied fully by Mg and Ti are 168 and 256 GPa, respectively. Considering the experimental uncertainties, these values are comparable to the bulk moduli for the MgO_6 octahedron in periclase (161 ± 5 GPa; Schreiber and Anderson 1966), and the TiO_6 octahedra in rutile (213 ± 47 GPa; Hazen and Finger 1981) and in ilmenite (289 ± 64 GPa; Wechsler and Prewitt 1984).

Similar to the response of octahedral volumes to pressure, all mean <M-O> bond lengths decrease linearly with increasing pressure, with an increase in the linear compressibility of the mean <M2-O> distance and a decrease in that of the mean <M1-O> distance in the more disordered structure. The linear compressibilities of the mean <M1-O> and <M2-O> bond lengths are 0.00243(5) and 0.00148(2) GPa^{-1}, respectively, in P600, and 0.00193(12) and 0.00163(7) GPa^{-1} in P1400. The linear compressibilities of the mean M-O bonds (β_m) are also strongly related to the Ti contents in the octahedral sites (X): The more Ti in a site, the less compressible the mean <M-O> bond, as illustrated in Figure 2. The relationship between β_m and X can be expressed by the equation: β_m (GPa^{-1}) = 0.00248(8) − 0.00108(4) *X*. From the above equation, the extrapolated β_m values for an octahedral site occupied fully by Mg and Ti are 0.00140 and 0.00248 GPa^{-1}, respectively.

TABLE 3. Interatomic distances (Å) and octahedral distortion indices for karrooite annealed at 600 and 1400 °C at various pressures

		Pressure (GPa)						
Sample	Bond	0.00	1.03	2.16	3.22	4.34	6.20	7.51
P600	M1-O1 ×2	2.048(2)	2.042(2)	2.037(2)	2.033(2)	2.028(2)	2.018(2)	2.013(2)
	M1-O2 ×2	1.990(3)	1.985(3)	1.977(3)	1.975(3)	1.967(3)	1.957(3)	1.949(4)
	M1-O3 ×2	2.204(3)	2.204(3)	2.195(3)	2.189(3)	2.186(3)	2.178(3)	2.169(3)
	Avg.	2.081	2.077	2.070	2.066	2.060	2.051	2.043
	*OV**	10.51(1)	10.47(1)	10.38(2)	10.32(1)	10.25(1)	10.15(1)	10.05(1)
	OQE	1.0952(5)	1.0941(5)	1.0931(5)	1.0926(5)	1.0920(6)	1.0899(6)	1.0891(6)
	OAV	256.8(5)	254.0(6)	251.7(6)	251.6(5)	249.6(6)	245.4(6)	243.4(6)
	M2-O1 ×1	2.014(2)	2.012(2)	2.008(2)	2.002(2)	2.000(2)	1.994(2)	1.990(2)
	M2-O2′ ×1	1.804(3)	1.801(3)	1.805(3)	1.797(3)	1.798(3)	1.793(3)	1.793(3)
	M2-O2 ×1	1.997(2)	1.994(3)	1.986(3)	1.987(3)	1.982(3)	1.980(3)	1.975(3)
	M2-O3 ×1	2.177(3)	2.173(3)	2.169(3)	2.164(3)	2.158(3)	2.152(3)	2.145(3)
	M2-O3′ ×2	1.938(1)	1.935(1)	1.931(1)	1.929(1)	1.926(1)	1.920(1)	1.917(1)
	Avg.	1.978	1.975	1.972	1.968	1.965	1.960	1.956
	OV	9.76(1)	9.73(1)	9.69(1)	9.63(1)	9.59(1)	9.53(1)	9.47(1)
	OQE	1.0408(3)	1.0401(3)	1.0397(3)	1.0397(3)	1.0393(3)	1.0383(3)	1.0381(3)
	OAV	125.4(4)	123.4(6)	122.3(4)	122.1(4)	121.2(4)	118.1(4)	117.8(4)
P1400	M1-O1 ×2	2.010(2)	2.007(2)	2.003(1)	1.997(2)	1.995(2)	1.987(2)	1.978(2)
	M1-O2 ×2	1.946(3)	1.935(3)	1.931(3)	1.924(3)	1.922(4)	1.915(4)	1.911(4)
	M1-O3 ×2	2.145(3)	2.137(3)	2.131(3)	2.140(3)	2.128(3)	2.122(4)	2.118(4)
	Avg.	2.034	2.026	2.021	2.020	2.015	2.008	2.002
	OV	10.11(2)	10.00(1)	9.94(2)	9.94(1)	9.86(1)	9.78(2)	9.73(2)
	OQE	1.0731(4)	1.0732(4)	1.0725(4)	1.0717(4)	1.0714(5)	1.0702(6)	1.0678(5)
	OAV	204.7(5)	205.1(5)	203.6(5)	200.9(5)	200.8(6)	197.9(8)	192.3(6)
	M2-O1 ×1	2.098(2)	2.090(2)	2.084(2)	2.081(2)	2.075(3)	2.065(3)	2.066(3)
	M2-O2′ ×1	1.857(3)	1.859(3)	1.855(3)	1.854(3)	1.850(3)	1.842(4)	1.836(4)
	M2-O2 ×1	1.986(3)	1.989(3)	1.983(3)	1.983(3)	1.976(4)	1.969(4)	1.969(4)
	M2-O3 ×1	2.164(3)	2.159(3)	2.157(3)	2.155(3)	2.153(4)	2.145(4)	2.146(4)
	M2-O3′ ×2	1.946(1)	1.943(1)	1.939(1)	1.933(1)	1.931(1)	1.924(1)	1.919(1)
	Avg.	1.999	1.997	1.993	1.990	1.986	1.978	1.976
	OV	10.08(1)	10.05(1)	9.99(1)	9.97(1)	9.91(1)	9.80(2)	9.78(2)
	OQE	1.0406(3)	1.0405(3)	1.0402(3)	1.0382(3)	1.0386(3)	1.0379(3)	1.0368(3)
	OAV	127.4(4)	126.8(4)	125.8(4)	119.4(4)	120.5(4)	118.7(5)	114.9(5)

Note: OV—octahedral volume (Å^3); *OQE*—octahedral quadratic elongation; *OAV*—octahedral angle variance (Robinson et al. 1971).

Unlike the compressibilities of mean <M-O> bond lengths, the linear compressibilities of individual M-O bond distances within an octahedron, however, are not a function of their magnitude. In fact, an opposite result has been observed for the M-O bonds within the M1 octahedron; namely, the shortest M1-O2 bond compresses most and the longest M1-O3 bond least. The M1-O2 bond length, whose room-pressure value is 1.990(3) Å in P600 and 1.946(3) Å in P1400 (Table 3), decreases by 2.1% and 1.8%, respectively, up to 7.51 GPa. Yet, the M1-O3 distances in P600 and P1400 at room pressure are 2.204(3) and 2.145(3) Å, respectively, but they decrease only by 1.6 and 1.3% in the same pressure range. This unexpected behavior at a first glance stems from the complex edge-sharing between M1 and M2 octahedra, each of them sharing six edges with neighboring octahedra. Specifically, each M1 octahedron shares two O2-O3 and four O1-O3 edges with the surrounding M2 octahedra, leaving the O2-O2 edge unshared (Fig. 3a). At room pressure, the M1-M2 separations across the O1-O3 edges are ~3.1 Å and those across the O2-O3 edges are ~3.2 Å. Given such a configuration, a decrease in the M1-O3 (or M1-O1) bond length will result in a shortening of the separations between one M1 and four M2 cations, which will increase the repulsion between them considerably. In contrast, a decrease in the M2-O2 distance will only involve the slight shortening of the separations between one M1 and two M2 cations. Because the M1-M2 separation across the O2-O3 edge is longer than that across the O1-O3 edge and the shortening of the M1-O2 bond length only results in a M1 cation moving closer to two M2 cations, rather than four, the compression of the short M1-O2 bond length is thus energetically more favorable than that of the long M1-O3 distance. For the same reason, the O2-O2 edge displays the greatest reduction of all O-O distances with increasing pressure, by 3.2% in both P600 and P1400 between room pressure and 7.51 GPa. A similar argument can account for the high-temperature data obtained by Wechsler (1977) for armalcolite [$(Mg_{0.5}Fe_{0.5})Ti_2O_5$] and by Morosin and Lynch (1972) for tieilite (Al_2TiO_5). In these two crystals, the repulsion between one M1 and four M2 cations across the shared O1-O3 edges is so strong that the M1-O2 bond distance decreases at higher temperatures.

Relative to the changes of the individual M-O bonds within the M1 octahedron with pressure, those within the M2 octahedron appear to be more ordering-dependent. In P600, the shortest M2-O2 bond length decreases by 0.6% between room pressure and 7.51 GPa and is the least compressible bond within the M2 octahedron, whereas the longest M2-O3 distance is the most compressible, shortening by 1.5%. However, in more disordered P1400,

TABLE 4. Interatomic angles of karrooite annealed at 600 and 1400 °C at various pressures

Sample	Angle	Pressure (GPa)						
		0.00	1.03	2.16	3.22	4.34	6.20	7.51
P600	O1-M1-O2	107.3(1)	107.2(1)	107.1(1)	107.1(1)	107.0(1)	106.8(1)	106.7(1)
	O1-M1-O3	77.6(1)	77.7(1)	77.8(1)	77.8(1)	77.9(1)	78.1(1)	78.2(1)
	O2-M1-O2′	86.8(2)	86.6(2)	86.6(2)	86.2(2)	86.2(2)	85.6(2)	85.6(2)
	O2-M1-O3	78.2(1)	78.3(1)	78.3(1)	78.4(1)	78.4(1)	78.7(1)	78.8(1)
	O3-M1-O3′	116.8(2)	116.9(2)	116.9(2)	116.9(2)	116.9(2)	116.9(2)	116.9(2)
	O1-M2-O2′	99.3(1)	99.4(1)	99.4(1)	99.3(1)	99.4(2)	99.4(2)	99.5(2)
	O1-M2-O3	102.3(1)	101.8(1)	101.8(1)	101.8(1)	101.6(1)	101.2(1)	101.2(2)
	O1-M2-O3′	84.9(1)	85.0(1)	84.9(1)	84.9(1)	85.0(1)	85.1(1)	84.9(1)
	O2-M2-O2′	79.8(1)	80.0(1)	80.1(1)	80.1(1)	80.2(1)	80.5(1)	80.6(2)
	O2′-M2-O3′	105.2(1)	105.1(1)	105.0(1)	105.0(1)	105.0(1)	104.8(1)	104.8(1)
	O2-M2-O3′	78.7(1)	78.8(1)	78.7(1)	78.8(1)	78.8(1)	78.9(1)	78.8(1)
	O2-M2-O3′	95.4(1)	95.2(1)	95.2(1)	95.2(1)	95.1(1)	95.0(1)	95.0(1)
	O3-M2-O3′	76.9(1)	76.9(1)	77.0(1)	77.0(1)	77.0(1)	77.1(1)	77.2(1)
	O3-O1-O3′	147.2(2)	147.3(2)	147.3(2)	147.3(2)	147.4(2)	147.4(2)	147.6(2)
	O1-O3-O3′	163.6(1)	163.6(1)	163.6(1)	163.6(1)	163.7(1)	163.7(1)	163.8(1)
P1400	O1-M1-O2	105.2(1)	105.3(1)	105.2(1)	105.1(1)	105.1(1)	105.0(1)	104.7(1)
	O1-M1-O3	78.7(1)	78.7(1)	78.7(1)	78.8(1)	78.8(1)	78.9(1)	79.1(1)
	O2-M1-O2′	86.9(2)	86.5(2)	86.5(2)	86.2(2)	86.1(2)	86.0(2)	85.3(2)
	O2-M1-O3	79.5(1)	79.6(1)	79.7(1)	79.9(1)	79.9(1)	80.0(2)	80.4(1)
	O3-M1-O3′	114.1(2)	114.3(2)	114.1(2)	113.9(2)	114.0(2)	113.9(2)	113.9(2)
	O1-M2-O2′	100.8(1)	100.5(1)	100.6(1)	100.5(1)	100.5(2)	100.7(2)	100.7(2)
	O1-M2-O3	100.5(1)	100.6(1)	100.6(1)	100.1(1)	100.2(2)	100.0(2)	99.5(2)
	O1-M2-O3′	81.3(1)	81.3(1)	81.3(1)	81.7(1)	81.6(1)	81.8(1)	81.8(1)
	O2-M2-O2′	80.6(1)	81.0(1)	80.9(1)	81.2(1)	81.2(2)	81.0(2)	81.3(2)
	O2′-M2-O3′	104.3(1)	104.3(1)	104.2(1)	103.9(1)	103.9(1)	103.8(1)	103.6(1)
	O2-M2-O3	78.2(1)	77.9(1)	77.9(1)	78.3(1)	78.1(1)	78.3(2)	78.4(1)
	O2-M2-O3′	98.4(1)	98.4(1)	98.4(1)	97.9(1)	98.1(1)	97.8(1)	97.8(1)
	O3-M2-O3′	79.0(1)	79.0(1)	79.1(1)	79.1(1)	79.2(1)	79.2(1)	79.3(1)
	O3-O1-O3′	153.5(2)	153.4(2)	153.4(2)	153.0(2)	152.9(2)	152.9(2)	153.0(2)
	O1-O3-O3′	166.8(1)	166.7(1)	166.7(1)	166.5(1)	166.5(1)	166.5(1)	166.5(1)

the shortest M2-O2 bond length, which decreases by 1.1% from room pressure to 7.51 GPa, is no longer the least compressible within the M2 octahedron; instead, the longest M2-O3 bond length becomes the least compressible bond, contracting by 0.8% in the same pressure range.

All octahedra in P600 and P1400 become progressively less distorted at higher pressures, as indicated by the octahedral quadratic elongation (QE) and angle variance (AV) (Robinson et al. 1971). Compared to the M1 octahedron, the M2 octahedron in both samples shows a great reduction in the AV value, but a small reduction in the QE value. Nevertheless, pressure appears to have stronger effects on the AV values of the two octahedra in P1400 than on those in P600: The respective AV values of the M1 and M2 octahedra in more ordered P600 decrease by 5.2 and 6.1% in the experimental pressure range, whereas those in P1400 decrease by 6.1 and 9.8%, despite the fact that the M1 octahedron in P1400 is far less distorted than that in P600 (Table 3). It is interesting to note that with increasing pressure the rates of decrease in the QE values for individual octahedra are also a linear function of the Ti contents in these sites: A site containing more Ti shows a smaller percentage decrease in the QE value, due primarily to the Ti^{4+}-O bond being stronger than the Mg^{2+}-O bond.

In the karrooite structure, the M1 and M2 octahedra share edges to form octahedral bands running parallel to the *b* axis (Fig. 3a). The configuration of these bands can be described by two kinking angles, i.e., the O3-O1-O3′ and O1-O3-O3′ angles. These two angles in karrooite and other pseudobrookite-type compounds have been found to vary with temperature (Wechsler 1977), composition (Smyth 1974; Wechsler et al. 1976; Brigatti et al. 1993), and cation order-disorder (Yang and Hazen 1998). For example, from room temperature to 1100 °C, the O3-O1-O3′ angle in a synthetic armalcolite increases by 7.3° (Wechsler 1977); the same angle increases linearly with increasing cation disorder from 147.2(2)° Å in P600 to 153.5(2)° Å in P1400. However, within the experimental uncertainties, the O3-O1-O3′ and O1-O3-O3′ angles in both P600 and P1400 are essentially independent of pressure (Table 4). Between room pressure and 7.51 GPa, the changes in the O-M-O angles in P600 range from 0 to 1.2°, with an average value of 0.5°, and those in P1400 range from 0.2 to 1.6°, with an average value of 0.6°. These results suggest that compression of the karrooite structure is not controlled by interatomic angle bending, but rather by the shortening of interatomic distances. This conclusion is consistent with Hazen and Finger (1985), who demonstrated that bond-angle bending and intermolecular changes cannot be major factors dominating compression of crystals with close-packed structures.

Yang and Hazen (1998) noted a close correlation between magnitudes of atomic displacement factors (B_{iso}) and cation disorder: With increasing cation disorder, B_{iso} values of all atoms increase. The B_{iso} factor of the O1 atom increases most, by ~60% from P600 to P1400. Yang and Hazen (1998) suggested two possibilities for the large B_{iso} value of O1 in the more disordered samples.

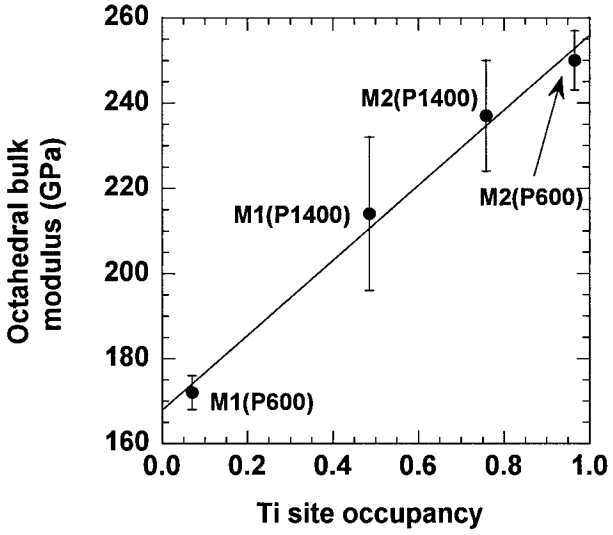

FIGURE 1. Octahedral bulk moduli in karrooite vs. the Ti site occupancies in the octahedral sites.

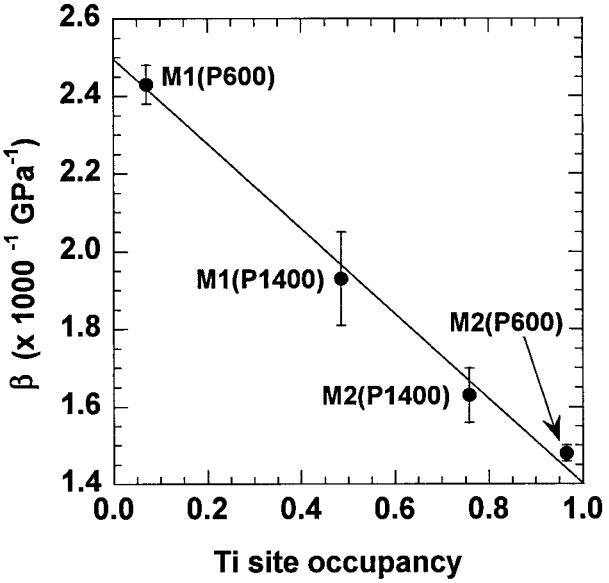

FIGURE 2. Linear compressibilties of the mean <M-O> bond lengths vs. the Ti site occupancies in the octahedral site.

(1) It may be a reflection of the increase in the atomic positional disorder at the O1 site due to the straightening of the O3-O1-O3′ angle, the O1 atom acting as a pivot point for the stretching of the octahedral bands running parallel to the *b* axis. (2) It could be a real representation of atomic thermal vibration as a consequence of compensation for an electron density distribution related to a local charge imbalance on O1. Because high pressure could measurably reduce atomic B_{iso} factors that result predominately from static positional disorder, but has little influence on B_{iso} parameters that primarily represent thermal vibration, our high-pressure data could provide information about the nature of the large B_{iso} factor of O1 in P1400. Within the experimental errors, the B_{iso} factor of O1 in P600 is virtually unchanged from room pressure to 7.51 GPa (Table 2), whereas that in P1400 reduces by ~36%. In fact, among all atoms in the two samples studied, only the O1 atom in P1400 exhibits an appreciable decrease in the B_{iso} value as pressure increases; the changes in the B_{iso} factors of all other atoms are insignificant. Accordingly, the relatively large B_{iso} factor of O1 in more disordered P1400 is likely to originate from static positional disorder at the O1 site.

Hazen and Yang (1997) showed that the linear compressibility of the *b* dimension in all four samples they studied is similar (~0.0024 GPa^{-1}), but the compressibilities of the *a* and *c* dimensions in P1400 are 10 and 7% greater, respectively, than those in P600. From the M1 and M2 octahedral linkage in the structure, they concluded that the compression along the *b* axis is always controlled by the average of compressibilities of one M1 and two M2 octahedra, regardless of the Mg-Ti distribution between the two different sites, whereas the compression along the *a* and *c* axes is determined principally by the compressibility of the M2 octahedra, which form continuous edge-shared octahedral layers parallel to the *a*–*c* plane (Fig. 3b). This conclusion is fully supported by our structure data. For instance, the average of bulk moduli of one M1 and two M2 octahedra for P600 is 224(6) GPa, whereas that for P1400 is 229(15) GPa, indicating that the two crystals should have similar compressibilities along the *b* axis.

The crystal structure of karrooite exhibits strong compression anisotropy, with the *b* direction about twice as compressible as *c*. The relative axial compression ratios are 1.58:2.02:1.00 for P600 and 1.63:1.85:1.00 for P1400. This observation is compared to the thermal expansion data measured by Bayer (1971) on karrooite, who found that the largest thermal expansion direction in the karrooite structure is along the *b* axis and the smallest along the *c* axis. The linear thermal expansion coefficient of the *b* axis is about seven times that of the *c* axis at 1020 °C. [Note: We corrected the unit-cell orientation and space group (*Cmcm*) used by Bayer (1971), which differ from this study]. The strong compression (or thermal expansion) anisotropy of the karrooite structure stems from the special kind of octahedral linkage. The greater compressibility along the *a* axis than along the *c* axis can be understood by the M2 octahedral linkage that forms the octahedral layers parallel to the *a*–*c* plane. As can be seen in Fig. 3b, each octahedron in the octahedral layer shares two edges with others to form a zigzag chain extending along the *c* axis and shares another one along the *a* axis with an octahedron in the adjacent chain. Apparently, these edge-shared zigzag chains become the load-bearing framework at high pressures, resulting in the smaller compression along the *c* axis than along the *a* axis. The *b* axis compression differs from the compression mechanism along the *a* or *c* axis, which is principally controlled by the high-pressure behavior of the M2 octahe-

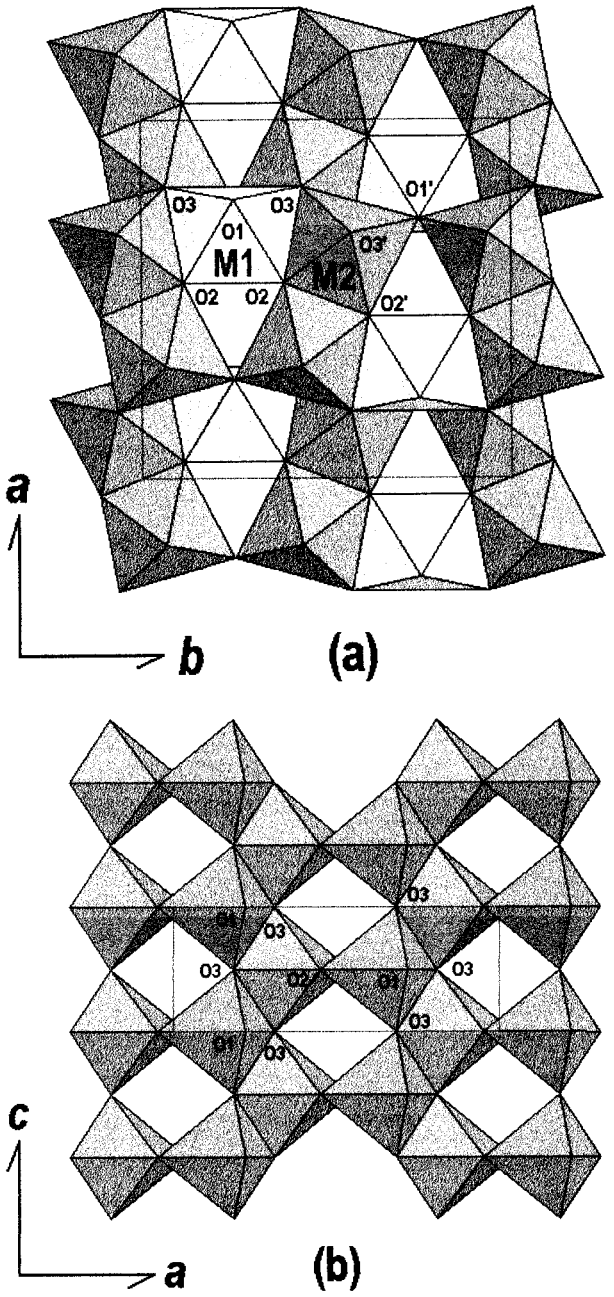

FIGURE 3. The karrooite structure: (**a**) viewed along *c*, showing the bands of the M1 and M2 octahedra, and (**b**) viewed along *b*, showing the edge-shared M2 octahedral layer. Note the zigzag chains running parallel to the *c* axis.

dra. Compression along the *b* axis involves both M1 and M2 octahedra (the structure along the *b* axis is characterized by the bands of the M1 and M2 octahedra). Because the M1 octahedra, which are preferentially occupied by Mg, are always softer than the M2 octahedra, the structure is thus expected to be more compressible along the *b* axis than along *a* or *c*.

CONCLUSIONS

We demonstrated in this study that cation order-disorder can significantly modify the high-pressure behavior of the karrooite structure. Based on the cation ordering data of Yang and Hazen (1998) and estimates of the dependence of the bulk moduli on ordering state (Hazen and Yang 1997), Ghiorso et al. (unpublished manuscript) showed that the Gibbs free energy of the disordered karrooite structure is always more positive than that of the ordered structure (due to the positive value of ΔV_{dis}, the unit-cell volume difference between the disordered and ordered phases), suggesting that there is a thermodynamic driving force for karrooite to become more ordered as pressure is increased at constant temperature. Pressure-induced atomic ordering has been observed in several crystalline phases, including many geologically important minerals (see the review by Hazen and Navrotsky 1996). Additional systematic studies on atomic order-disorder, compressibility, and crystal chemistry of these phases are essential to obtain more realistic equations of state for mantle phases that exhibit ordering-dependent properties and to gain detailed insights into the effects of pressure on cation ordering.

ACKNOWLEDGMENTS

We thank N. Boctor for his kind help in the synthesis and quenching experiments of the $MgTi_2O_5$ crystals. X-ray diffraction work and postdoctoral fellowship to H.Y. at the Geophysical Laboratory are supported by NSF grant EAR-9218845, the Center for High Pressure Research, and by the Carnegie Institution of Washington.

REFERENCES CITED

Bayer, G. (1971) Thermal expansion and stability of pseodobrookite-type compounds, Me_3O_5. Journal of Less Common Metals, 24, 129–138.

Becker, P.J. and Coppens, P. (1975) Extinction within the limit of validity of the Darwin transfer equations: III. Non-spherical crystals and anisotropy of extinction. Acta Crystallographica, A31, 417–425.

Brigatti, M.F., Contini, S., Capedri, S., and Poppi, L. (1993) Crystal chemistry and cation ordering in pseudobrookite and armalcolite from Spanish lamproites. European Journal of Mineralogy, 5, 73–84.

Brown, N.E. and Navrotsky, A. (1989) Structural, thermodymanic, and kinetic aspects of disordering in the pseudobrookite-type compound karrooite, $MgTi_2O_5$. American Mineralogist, 74, 902–912.

Finger, L.W. and Prince, E. (1975) A system of FORTRAN IV computer programs for crystal structure computations. National Bureau of Standards Technology Note, 854.

Finger, L.W. and King, H. (1978) A revised method of operation of the single-crystal diamond cell and refinement of the structure of NaCl at 32 kbar. American Mineralogist, 63, 337–342.

Hazen, R.M. (1993) Comparative compressibilities of silicate spinels: Anomalous behavior of $(Mg,Fe)_2SiO_4$. Science, 259, 206–209.

Hazen, R.M. and Finger, L.W. (1981) Bulk Moduli and high-pressure crystal structures of rutile-type compounds. Journal of Physics and Chemistry of Solids, 42, 143–151.

———(1985) Crystals at high pressure. Scientific American, 252, 110–117.

Hazen, R.M. and Navrotsky, A. (1996) Effects of pressure on order-disorder reactions. American Mineralogist, 81, 1021–1035.

Hazen, R.M. and Yang, H. (1997) Cation disorder increases the compressibilty of pseudobrookite-type $MgTi_2O_5$. Science, 277, 1965–1967.

Ibers, J.A. and Hamilton, W.C., Eds. (1974) International tables for X-ray crystallography, vol. IV, 366 p. Kynoch, Birmingham, U.K.

King, H.E. and Finger, L.W. (1979) Diffracted beam crystal centering and

its application to high pressure crystallography. Journal of Applied Crystallography, 12, 374–378.

Lehmann, M.S. and Larsen, F.K. (1974) A method for location of the peaks in step-scan-measured Bragg reflexions. Acta Crystallographica, A30, 580–584.

Lind, M.D. and Housley, R.M. (1972) Crystallization studies of lunar igneous rocks: Crystal structure of synthetic armalcolite. Science, 175, 521–523.

Mao, H.K., Xu, J., and Bell, P.M. (1986) Calibration of the ruby pressure gauge to 800 kbar under quasi-hydrostatic conditions. Journal of Geophysical Research, 91, 4673–4676.

Morosin, B. and Lynch, R.W. (1972) Structure studies of Al_2TiO_5 at room temperature and at 600 °C. Acta Crystallographica, B28, 1040–1046.

Navrotsky, A. (1975) Thermodynamics of formation of some compounds with the pseudobrookite structure and of the $FeTi_2O_5$-Ti_3O_5 solid solution series. American Mineralogist, 60, 249–256.

Pauling, L. (1930) The crystal structure of pseudobrookite. Zeitschrift für Kristallographie, 73, 97–112.

Robinson, K., Gibbs, G.V., and Ribbe, P.H. (1971) Quadratic elongation: A quantitative measure of distortion in coordination polyhedra. Science, 172, 567–570.

Schreiber, E. and Anderson, O.L. (1966) Pressure derivatives of the sound velocity of polycrystalline alumina. Journal of American Ceramics Society, 49, 184–190.

Smyth, J.R. (1974) The crystal chemistry of armalcolite from Apollo 17. Earth and Planetary Science Letters, 24, 262–270.

Virgo, D. and Huggins, F.E. (1975) Cation distributions in some compounds with the pseodobrookite structure. Carnegie Institution of Washington Year Book, 74, 585–590.

Wechsler, B.A. (1977) Cation distribution and high-temperature crystal chemistry of armalcolite. American Mineralogist, 62, 913–920.

Wechsler, B.A. and Navrotsky, A. (1984) Thermodynamic and structural chemistry of compounds in the system MgO-TiO_2. Journal of Solid State Chemistry, 55, 165–180.

Wechsler, B.A. and Prewitt, C.T. (1984) Crystal structure of ilmenite ($FeTiO_3$) at high temperature and at high pressure. American Mineralogist, 69, 176–185.

Wechsler, B.A. and Von Dreele, R.B. (1989) Structure refinements of Mg_2TiO_4, $MgTiO_3$ and $MgTi_2O_5$ by time-of-flight neutron powder diffraction. Acta Crystallographica, B45, 542–549.

Wechsler, B.A., Prewitt, C.T., and Papike, J.J. (1976) Chemistry and structure of lunar and synthetic armalcolite. Earth and Planetary Science Letters, 29, 91–103.

Yang, H. and Hazen, R.M. (1998) Crystal chemistry of cation order-disorder in pseudobrookite-type $MgTi_2O_5$. Journal of Solid State Chemistry, 138, 238–244.

Manuscript received February 9, 1998
Manuscript accepted August 27, 1998
Paper handled by Simon A.T. Redfern